AIP | Journal of Applied Physics

Analysis of periodic metallic nano-slits for efficient interaction of terahertz and optical waves at nano-scale dimensions

Bing-Yu Hsieh and Mona Jarrahi

Citation: J. Appl. Phys. **109**, 084326 (2011); doi: 10.1063/1.3567909
View online: http://dx.doi.org/10.1063/1.3567909
View Table of Contents: http://jap.aip.org/resource/1/JAPIAU/v109/i8
Published by the AIP Publishing LLC.

Analysis of periodic metallic nano-slits for efficient interaction of terahertz and optical waves at nano-scale dimensions

Bing-Yu Hsieh and Mona Jarrahi
Department of Electrical Engineering and Computer Science, University of Michigan, 1301 Beal Ave, Ann Arbor, Michigan 48109, USA

(Received 7 January 2011; accepted 22 February 2011; published online 21 April 2011)

We analyze the unique property of periodic arrays of subwavelength metallic slits to allow extraordinary electromagnetic transmission at multiple frequency bands. The diffraction limit in periodic arrays of subwavelength metallic slits is mitigated by excitation of surface waves which assist efficient coupling of a transverse magnetic–polarized incident electromagnetic wave into the TEM waveguide modes of the subwavelength slab waveguides formed by metallic slits. By investigating the geometry dependence of the electromagnetic guided modes supported by periodic arrays of subwavelength metallic slits, we present the design of a periodic array of metallic nanoslits which enables efficient interaction of terahertz and optical waves at nanoscale dimensions. © *2011 American Institute of Physics*. [doi:10.1063/1.3567909]

I. INTRODUCTION

Transmission enhancement of electromagnetic waves through subwavelength metallic apertures has attracted increasing interest[1–5] since the first demonstration of extraordinary optical transmission through subwavelength arrays of holes.[6] It has offered many unique functionalities for routing and manipulating electromagnetic waves,[7] enabling imaging and spectroscopy techniques with improved spatial resolution,[8,9] ultrafast and compact photodetectors[10,11] and modulators,[12,13] wavelength tunable filters, higher efficiency solar cells,[14,15] and enhanced nonlinear processes in ultracompact device geometries.[16,17]

In this work, we analyze the property of periodic arrays of subwavelength metallic slits to allow extraordinary electromagnetic transmission at multiple frequency bands. Based on this analysis, we present the design of a periodic array of metallic nanoslits which enables efficient interaction of terahertz and optical waves at nanoscale dimensions. Such unique capability would significantly improve the performance of existing photoconductive terahertz sources, detectors, and mixers and enable fundamental studies on light–matter interaction at a very fundamental level such as single molecule spectroscopy.[18–21]

II. METHODOLOGY

Figure 1 illustrates the cross-sectional view of the subwavelength metallic slits supporting multiple subwavelength guided modes. Because of the two-dimensional geometry of the metallic slits, their interaction with electromagnetic waves is strongly polarization dependent. For a transverse electric (TE)–polarized electromagnetic excitation (electric field in y direction), the metallic slits only support evanescent modes. For a transverse magnetic (TM)–polarized electromagnetic excitation (magnetic field in y direction), in addition to evanescent modes, the subwavelength slab waveguides formed by the metallic slits also support TEM electromagnetic guided modes at wavelengths larger than the slit periodicity, d. Therefore, efficient electromagnetic power transmission through the metallic slits can be achieved.[22,23] In this section, the power transmissivity of a TM-polarized incident electromagnetic wave through the metallic slits into a dielectric substrate, as a function of slit geometry (a, h, d) and electromagnetic wavelength is analytically derived.

For a normally incident TM–polarized electromagnetic excitation, the magnetic field in regions 1 ($z \geq 0$) and 3 ($z \leq -h$) are calculated as:

$$\tilde{H}_y^{(1)} = -\sum_{p=-\infty}^{\infty} \left[u_{1,p} e^{i\alpha_p z} e^{iG_p x} + r_{1,p} e^{-i\alpha_p z} e^{iG_p x}\right] \quad (1)$$

$$\tilde{H}_y^{(3)} = -\sum_{p=-\infty}^{\infty} t_p e^{i\alpha_{\text{psub}}(z+h)} e^{iG_p x} \quad (2)$$

where $u_{1,p}$ is the amplitude of the forward-propagating pth diffraction mode on the periodic subwavelength metallic slits, $r_{1,p}$ is the amplitude of the backward-propagating pth diffraction mode from the top of the periodic subwavelength metallic slits, t_p is the amplitude of the transmitted pth diffraction mode into the dielectric substrate. $G_p = 2\pi p/d$ is the parallel momentum along metal surface, k is the momentum of the incident wave, $\alpha_p = \sqrt{(k^2 - G_p^2)}$ is the momentum of electromagnetic wave in the z direction, ϵ_{sub} is the substrate permittivity, k_{sub} is the electromagnetic momentum in the dielectric substrate, and $\alpha_{\text{psub}} = \sqrt{(k_{\text{sub}}^2 - G_p^2)}$ is the z component of electromagnetic momentum in the dielectric substrate. It should be noted that, based on the assumption of high electromagnetic attenuation along the substrate thickness, the presented analysis neglects the reflected signal from the back of the dielectric substrate.

The electric field in regions 1 and 3 has components in the x and z directions which are calculated using Maxwell's equation $\nabla \times \tilde{H} = \varepsilon \frac{\partial \tilde{E}}{\partial t}$ ($\tilde{E}_x = \frac{1}{j\omega\varepsilon}\frac{\partial \tilde{H}_y}{\partial z}$, $\tilde{E}_z = \frac{1}{j\omega\varepsilon}\frac{\partial \tilde{H}_y}{\partial x}$):

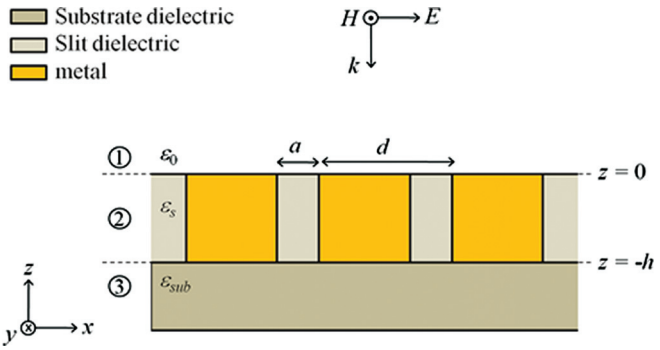

FIG. 1. (Color) Schematic view of the subwavelength metallic slits supporting multiple subwavelength guided modes.

$$\tilde{E}_x^{(1)} = \sum_{p=-\infty}^{\infty} \left[\frac{\alpha_p}{\omega\varepsilon_0} u_{1,p} e^{i\alpha_p z} e^{iG_p x} - \frac{\alpha_p}{\omega\varepsilon_0} r_{1,p} e^{-i\alpha_p z} e^{iG_p x} \right] \quad (3)$$

$$\tilde{E}_x^{(3)} = \sum_{p=-\infty}^{\infty} \frac{\alpha_{\text{psub}}}{\omega\varepsilon_{\text{sub}}} t_p e^{i\alpha_{\text{psub}}(z+h)} e^{iG_p x}. \quad (4)$$

The magnetic field in region 2 ($0 \geq z \geq -h$) is calculated as:

$$\tilde{H}_y^{(2)} = -u_2 e^{ik_s z} - r_2 e^{-ik_s(z+h)} \quad (5)$$

where u_2 and r_2 are the magnetic field amplitudes of the forward and backward propagating TEM modes in the slits with permittivity of ε_s, and k_s is the electromagnetic momentum in the metallic slits. The corresponding x component of the electric field in region 2 is calculated using Maxwell's equation:

$$\tilde{E}_x^{(2)} = \frac{k_s}{\omega\varepsilon_s} u_2 e^{ik_s z} - \frac{k_s}{\omega\varepsilon_s} r_2 e^{-ik_s(z+h)}. \quad (6)$$

The boundary condition (continuity of the tangential field components) at $z = 0$ and $z = -h$ is used to find the transmissivity of an incident TM–polarized electromagnetic wave into the dielectric substrate: At $z = 0$,

$$\text{At } z = 0, \quad \tilde{H}_y^{(1)} = \tilde{H}_y^{(2)} \text{ and } \tilde{E}_x^{(1)} = \tilde{E}_x^{(2)} :$$

$$\sum_{p=-\infty}^{\infty} \left[u_{1,p} e^{iG_p x} + r_{1,p} e^{iG_p x} \right] = u_2 + r_2 e^{-ik_s h} \quad (7)$$

$$\sum_{p=-\infty}^{\infty} \left[\frac{\alpha_p}{\omega\varepsilon_0} u_{1,p} e^{iG_p x} - \frac{\alpha_p}{\omega\varepsilon_0} r_{1,p} e^{iG_p x} \right] = \frac{k_s}{\omega\varepsilon_s} u_2 - \frac{k_s}{\omega\varepsilon_s} r_2 e^{-ik_s h}. \quad (8)$$

$$\text{At } z = -h, \quad \tilde{H}_y^{(2)} = \tilde{H}_y^{(3)} \quad \text{and} \quad \tilde{E}_x^{(2)} = \tilde{E}_x^{(3)}$$

$$\sum_{p=-\infty}^{\infty} t_p e^{iG_p x} = u_2 e^{-ik_s h} + r_2 \quad (9)$$

$$\sum_{p=-\infty}^{\infty} \frac{\alpha_{\text{psub}}}{\omega\varepsilon_{\text{sub}}} t_p e^{iG_p x} = \frac{k_s}{\omega\varepsilon_s} u_2 e^{-ik_s h} - \frac{k_s}{\omega\varepsilon_s} r_2. \quad (10)$$

By integrating both sides of Eqs. (7) and (9) over one period of the metallic slits:

$$\sum_{p=-\infty}^{\infty} \left[u_{1,p} + r_{1,p} \right] g_p = u_2 + r_2 e^{-ik_s h} \quad (11)$$

$$\sum_{p=-\infty}^{\infty} t_p g_p e^{-iG_p d/2} = u_2 e^{-ik_s h} + r_2 \quad (12)$$

where,

$$g_p = \frac{\sin(G_p a/2)}{G_p a/2}.$$

Also, by multiplying both sides of Eqs. (8) and (10) by $e^{-G_{p'}x}$ and integrating over one period of the metallic slits, the next set of boundary conditions can be calculated. It should be noted that the electric field at the metal–air boundary is calculated using the metal surface impedance η ($\tilde{E}_x = \eta \tilde{H}_y$).

$$\frac{\alpha_p}{\omega\varepsilon_0}(u_{1,p} - r_{1,p}) = \frac{a}{d} g_p \frac{k_s}{\omega\varepsilon_s}(u_2 - r_2 e^{-ik_s h}) + \eta(u_{1,p} + r_{1,p}) \quad (13)$$

$$\frac{\alpha_{\text{psub}}}{\omega\varepsilon_{\text{sub}}} t_p = \frac{a}{d} g_p e^{-iG_p d/2} \frac{k_s}{\omega\varepsilon_s}(u_2 e^{-ik_s h} - r_2) + \eta t_p. \quad (14)$$

By eliminating the variables $r_{1,p}$, u_2, and r_2, the transmission amplitude t_p for the pth diffraction order is calculated. It should be noted that for an obliquely incident TM–polarized electromagnetic wave, the transmission amplitude for the pth diffraction order is calculated by modifying the electromagnetic momentum along the metallic slit surface, $G_p = k_x + 2\pi p/d$, where k_x is the incident electromagnetic momentum along the x axis. Except for the zeroth order diffraction mode, other excited surface diffraction modes exhibit an imaginary wave momentum in the dielectric substrate and air (α_{psub} and α_p) and are therefore evanescent. Therefore, the amplitude of guided modes through the metallic slits into the dielectric substrate is calculated as

$$t_0 = \frac{4\frac{a}{d}\frac{k_s}{\omega\varepsilon_s}}{\left(\frac{k_{sub}}{\omega\varepsilon_{sub}} - \eta\right)\left(1 + \eta\frac{\omega\varepsilon_0}{k}\right)} \times \frac{e^{-jk_s h}}{(1+\Phi_1)(1+\Phi_2) - e^{-j2k_s h}(1-\Phi_1)(1-\Phi_2)} \quad (15)$$

where

$$\Phi_1 = \sum_{p=-\infty}^{\infty} \frac{a}{d} g_p^2 \frac{\frac{k_s}{\omega\varepsilon_s}}{\frac{\alpha_p}{\omega\varepsilon_s} + \eta}, \quad \Phi_2 = \sum_{p=-\infty}^{\infty} \frac{a}{d} g_p^2 \frac{\frac{k_s}{\omega\varepsilon_s}}{\frac{\alpha_{psub}}{\omega\varepsilon_{sub}} - \eta}.$$

III. RESULTS AND DISCUSSION

Figure 2(a) illustrates predictions of the presented model [Eq. (15)] to estimate the power transmission spectrum of a TM–polarized electromagnetic wave through a periodic array of subwavelength metallic slits as a function of slit

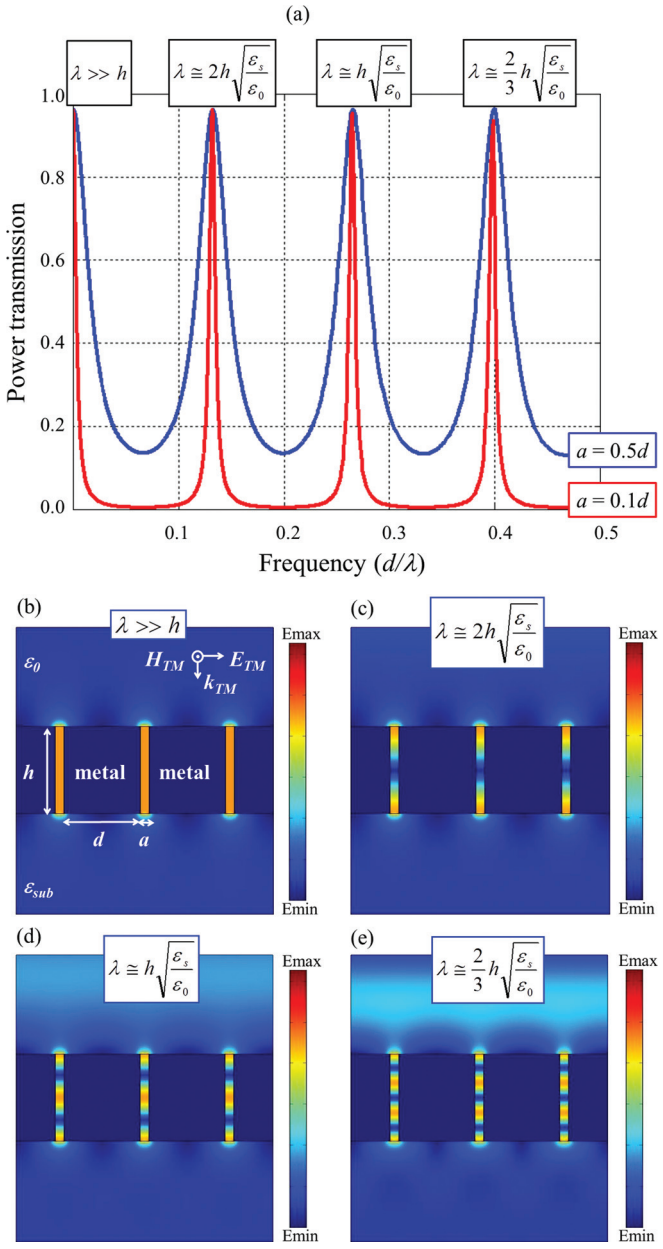

FIG. 2. (Color) (a) Transmission spectrum of a TM-polarized electromagnetic wave through a periodic array of subwavelength metallic slits ($h = 1.2d$ and $a = 0.1d$, $0.5d$) on a dielectric substrate, showing multiple guided modes. Silicon and silicon dioxide are used as the slit and substrate dielectrics. Perfect metals with infinite permittivity are used in this analysis to keep the generality of our theoretical model (Eq. 15) at an arbitrary wavelength. Color map of the electric field density of a TM-polarized electromagnetic wave interacting with the periodic array of subwavelength metallic slits ($h = 1.2d$ and $a = 0.1d$) at the 1st, 2nd, 3rd, and 4th guided mode wavelengths supported by the metallic slits, as in (b), (c), (d), and (e). The electric field distribution profiles correspond to the TEM modes supported by the subwavelength slab waveguides formed by the periodic array of metallic slits. COMSOL multiphysics package is used to calculate the electric field density of each guided mode.

geometry. For this analysis, silicon and silicon dioxide are used as the slit and substrate dielectrics. Slit geometric parameters are set to $h = 1.2d$ and $a = 0.1d$, $0.5d$ (d: slit periodicity). Also, perfect metals with infinite permittivity are used to keep the generality of our theoretical model at an arbitrary wavelength.

Our calculations indicate several guided modes at wavelengths much larger than the slit periodicity, d, with a cutoff wavelength of $\lambda_{\text{cutoff}} \cong d\sqrt{\varepsilon_{\text{sub}}/\varepsilon_0}$. The first guided mode is at the wavelength range much larger than the slit height ($\lambda \gg h$), and the rest of guided modes are at the resonant wavelengths of the subwavelength slab waveguide formed by the metallic slits, $\lambda_{\text{guided}}^{(n)} \cong 2h\sqrt{\varepsilon_s/\varepsilon_0}/n$ ($n = 1, 2, \ldots$). Because of the nonresonant nature of the first guided mode, the maximum power transmission of the first guided mode into the dielectric substrate, 61|560, is limited by the reflection at the substrate–air interface.

$$\xi = \frac{4\sqrt{\varepsilon_0\varepsilon_{\text{sub}}}}{\left(\sqrt{\varepsilon_0} + \sqrt{\varepsilon_{\text{sub}}}\right)^2}. \tag{16}$$

In the meantime, depending on the metallic slit geometry, the maximum power transmission of the resonant TEM guided modes into the dielectric substrate can be as high as 100%.

The COMSOL multiphysics package is used to calculate the electric field density of a TM–polarized electromagnetic wave interacting with the periodic array of subwavelength metallic slits. Slit geometric parameters used for this calculation are set to $h = 1.2d$ and $a = 0.1d$ (d: slit periodicity). Figures 2(b)–2(e), show the color map of the calculated electric field density at the 1st, 2nd, 3rd, and 4th guided mode wavelengths supported by the metallic slits. The electric field distribution profiles confirm that the guided modes through the periodic arrays of subwavelength metallic slits correspond to the TEM resonance modes supported by the subwavelength slab waveguides formed by the metallic slits. They show how the TM–polarized electromagnetic field lines are bent on top of the periodic arrangements of metallic slits to achieve high power transmission through the subwavelength slit regions into the underlying dielectric substrate.

As the results predict, the subwavelength metallic slit geometry can be specifically designed to support guided modes at wavelength ranges that are orders of magnitude far from each other. We have used this unique capability to design subwavelength metallic slit geometries that support guided modes at terahertz and optical wavelength ranges. In order to allow the first and second guided modes to fall in the terahertz and optical wavelength ranges, the selected slit height should be much smaller than the terahertz wavelength ($h << \lambda_{\text{THz}}$) and satisfy $h \cong 0.5\lambda_{\text{opt}}\sqrt{\varepsilon_0/\varepsilon_s}$. Additionally, the supported optical and terahertz guided modes should be at wavelengths larger than the cutoff wavelength ($d < \lambda_{\text{opt}}\sqrt{\varepsilon_0/\varepsilon_{\text{sub}}}$). These requirements necessitate the use of nanoscale metallic slits in order to support guided modes at terahertz and optical wavelengths simultaneously. The inherent trade-off between the bandwidth and field intensity enhancement of guided modes inside the subwavelength metallic slits should be taken into account to select a proper slit aspect ratio, d/a. While the transmission bandwidth of each guided mode is inversely proportional to the slit aspect ratio, d/a, the intensity enhancement of the transmitted electric field inside the subwavelength metallic slits has a quadratic dependence on the slit aspect ratio d/a.

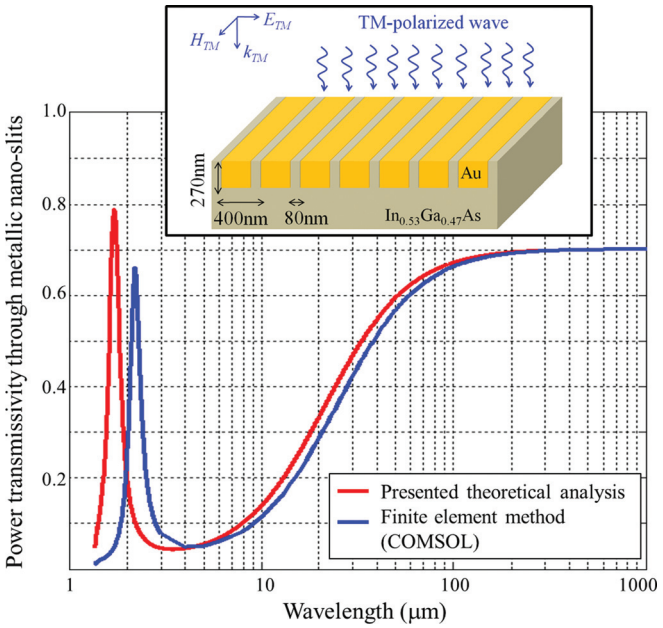

FIG. 3. (Color) Periodic arrays of metallic nanoslits designed to efficiently couple terahertz and optical electromagnetic waves into the nanoscale $In_{0.53}Ga_{0.47}As$ semiconductor regions, and the transmitted power into the nanoscale semiconductor regions calculated by the presented theoretical analysis (red curve) and the finite element method (blue curve).

Figure 3 shows a periodic array of metallic nanoslits designed for coupling TM–polarized terahertz and optical waves into the nanoscale $In_{0.53}Ga_{0.47}As$ semiconductor regions inside the nanoslits. In spite of two orders of magnitude difference between the terahertz and optical wavelengths, more than 70% of terahertz ($\lambda > 300$ μm) and optical (1500 nm $> \lambda >$ 1600 nm) power are predicted to couple into the nanoscale $In_{0.53}Ga_{0.47}As$ semiconductor regions sandwiched between the metallic slits. Figure 3 also shows the calculated power transmission spectrum of a normally incident TM–polarized electromagnetic wave into the nanoscale $In_{0.53}Ga_{0.47}As$ semiconductor regions inside the nanoslits using a finite element method solver (COMSOL package). The experimental complex permittivity of Au from literature is used for the finite element method simulation.[24] Predictions of the presented theoretical analysis and the finite element method solver perfectly match at the terahertz wavelength range. Slight differences between the wavelength and power transmissivity of the optical guided mode are associated with the extension of optical guided mode into the air, substrate, and metal regions compared to the boundary conditions considered in the presented theoretical model. This leads to a longer effective resonance length and higher attenuation for the optical TEM guided mode.

The choice of $In_{0.53}Ga_{0.47}As$ for the slit and substrate dielectrics in the analyzed array of metallic nanoslits is due to the high absorption coefficient of $In_{0.53}Ga_{0.47}As$ at standard telecom wavelengths. Additionally, the specific fractions of In and Ga in $In_{0.53}Ga_{0.47}As$ makes this semiconductor lattice match to InP, enabling growth of high-quality crystalline $In_{0.53}Ga_{0.47}As$ on InP substrates. As a result, the analyzed periodic array of metallic nanoslits could significantly enhance the efficiency of photoconductive terahertz sources, detectors, and mixers pumped at standard telecom wavelengths.

IV. CONCLUSION

Theoretical analysis of electromagnetic interaction with periodic arrays of subwavelength metallic slits indicates the existence of several electromagnetic guided modes at wavelengths much higher than metallic slit periodicity. Normally, electromagnetic coupling into subwavelength dimensions is limited by the diffraction limit. However, using periodic arrays of subwavelength metallic slits mitigates this limitation by excitation of surface waves which assist efficient coupling of a TM–polarized incident electromagnetic wave into the TEM waveguide modes of the subwavelength slab waveguides formed by the metallic slits. Theoretical analysis shows that the electromagnetic guided modes supported by periodic arrays of subwavelength metallic slits are strongly geometry dependent. Based on this analysis, we have designed a periodic array of metallic nanoslits that supports subwavelength TEM guided modes at terahertz and optical frequencies, enabling efficient interaction of terahertz and optical waves at nanoscale dimensions. Additional advantages of the designed array of nanoslits are the efficient interaction of optical and terahertz waves at deep subwavelength device active regions (less than $\lambda_{THz}/1000$), over a broad terahertz wavelength range ($h \ll \lambda_{THz}$) and a large device active area. Such capabilities would significantly improve the performance of existing photoconductive terahertz sources, detectors, and mixers.

ACKNOWLEDGMENTS

The authors gratefully acknowledge the financial support from DARPA Young Faculty Award (Award #064506), and discussions with Prof. Jung Tsung Shen, Washington University in St. Louis.

[1]J. B. Pendry, L. Martin-Moreno, and F. J. Garcia-Vidal, Science **305**, 847 (2004).
[2]A. P. Hibbins, B. R. Evans, and J. R. Sambles, Science **308**, 670 (2005).
[3]S. S. Akarca-Biyikli, I. Bulu, and E. Ozbay, Appl. Phys. Lett. **85**, 1098 (2004).
[4]H. J. Lezec, A. Degiron, E. Devaux, R. A. Linke, L. Martin-Moreno, F. J. Garcia-Vidal, and T. W. Ebbesen, Science **297**, 820 (2002).
[5]E. Ozbay, Science **311**, 189 (2006).
[6]T. W. Ebbesen, H. J. Lezec, H. F. Ghaemi, T. Thio, and P. A. Wolff, Nature **391**, 667 (1998).
[7]J. A. Schuller, E.S. Barnard, W. Cai, Y. C. Jun, J. S. White, and M. L. Brongersma, Nature Mater. **9**, 193 (2010).
[8]A. Hartschuh, E. J. Sanchez, X. S. Xie, and L. Novotny, Phys. Rev. Lett. **90**, 095503 (2003).
[9]H. Frey, S. Witt, K. Felderer, and R. Guckenberger, Phys. Rev. Lett. **93**, 200801 (2004).
[10]T. Ishi, T. Fujikata, K. Makita, T. Baba, and K. Ohashi, Jpn. J. Appl. Phys. **44**, 364–366 (2005).
[11]L. Tang, S. E. Kocabas, S. Latif, A. K. Okyay, D-S. Ly-Gagnon, K. C. Saraswat, and D. A. B. Miller, Nature Photon. **2**, 226 (2008).
[12]W. Cai, J. S. White, and M. L. Brongersma, Nano Lett. **9**, 4403 (2009).
[13]K. F. MacDonald, Z. L. Sámson, M. I. Stockman, and N. I. Zheludev, Nature Photon. **3**, 55 (2009).
[14]H. A. Atwater and A. Polman, Nature Mater. **9**, 205 (2010).
[15]R. A. Pala, J. White, E. Barnard, J. Liu, and M. L. Brongersma, Adv. Mater. **21**, 3504 (2009).

[16]S. Kim, J. Jin, Y.-J. Kim, I.-Y. Park, Y. Kim, and S.-W. Kim, Nature **453**, 757 (2008).
[17]J. A. H. Van Nieuwstadt, M. Sandtke, R. H. Harmsen, F. B. Segerink, J. C. Prangsma, S. Enoch, and L. Kuipers, Phys. Rev. Lett. **97**, 146102 (2006).
[18]E. R. Brown, *Terahertz Sensing Technology **1**: Electronic Devices and Advanced Systems Technology*, edited by D. L. Woolard, W. R. Loerop, and M. S. Shur (World Scientific, Singapore, 2003).
[19]C. W. Berry and M. Jarrahi, in Proceedings of the Conference on Lasers and Electro-Optics, San Jose, CA, 16–21 May 2010.
[20]S. Kuhn, U. Hakanson, L. Rogobete, and V. Sandoghdar, Phys. Rev. Lett. **97**, 017402 (2006).
[21]T. H. Taminiau, F. D. Stefani, F. B. Segerink, and N. F. Van Hulst, Nature Photon. **2**, 234 (2008).
[22]P. B. Catrysse, G. Veronis, H. Shin, J. T. Shen, and S. Fan, Appl. Phys. Lett. **88**, 031101 (2006).
[23]J. T. Shen and P. M. Platzman, Phys. Rev. B **70**, 035101 (2004).
[24]D. R. Lide, *Handbook of Chemistry and Physics*, 84th ed. (CRC, Cleveland, OH, 2003–2004).